NASA Technical Paper 3229

1992

Open-Loop Characteristics of Magnetic Suspension Systems Using Electromagnets Mounted in a Planar Array

Nelson J. Groom
Langley Research Center
Hampton, Virginia

Colin P. Britcher
Old Dominion University
Norfolk, Virginia

National Aeronautics and Space Administration

Office of Management

Scientific and Technical Information Program

Contents

Abstract

The open-loop characteristics of a Large-Gap Magnetic Suspension System (LGMSS) were investigated and numerical results are presented. The LGMSS considered provides five-degree-of-freedom control. The suspended element is a cylinder that contains a core composed of permanent magnet material. The magnetic actuators are air core electromagnets mounted in a planar array. Configurations utilizing five, six, seven, and eight electromagnets were investigated and all configurations were found to be controllable from coil currents and observable from suspended-element positions. Results indicate that increasing the number of coils has an insignificant effect on mode shapes and frequencies.

Introduction

This paper describes the open-loop characteristics of a Large-Gap Magnetic Suspension System (LGMSS). The LGMSS is a conceptual design for a ground-based experiment that can be used to investigate the technology issues associated with magnetic suspension at large gaps, accurate suspended-element control at large gaps, and accurate position sensing at large gaps (ref. 1). This technology is applicable to future efforts that range from magnetic suspension of wind-tunnel models to advanced spacecraft experiment isolation and pointing systems. The LGMSS considered provides five-degree-of-freedom control. The suspended element is a cylinder that contains a core composed of permanent magnet material. The magnetic actuators are air core electromagnets mounted in a planar array. In reference 2 an LGMSS configuration using five electromagnets was described and an analytical model of the configuration was developed. This analytical model was used in reference 3 to investigate two LGMSS control approaches. In reference 3 the simplifying assumption was made that the change in field and field gradients with respect to suspended-element displacements was negligible. The purpose of this paper is to investigate the open-loop characteristics of the LGMSS with the change in field and field gradients included to determine if they introduce any unusual stability problems. In addition to the minimum five-coil configuration, configurations utilizing six, seven, and eight coils are also investigated to determine the feasibility of independently controlling the field component that determines the magnitude of the highest open-loop frequencies. Each configuration is described, and values of field components generated by the electromagnets at the location of the suspended core are presented. The method of calculating field components is discussed in the appendix.

Symbols

$\mathcal{A}$	system matrix (state-space representation)
$\mathcal{B}$	input matrix (state-space representation)
$\mathbf{B}$	magnetic flux density vector, T
$[\partial \mathbf{B}]$	matrix of field gradients, T/m
$\mathbf{F}$	total force vector on suspended element, N
$\mathbf{F}_c$	magnetic force vector on suspended element, N
$\mathbf{F}_d$	disturbance force vector on suspended element, N
$\mathbf{F}_g$	gravitational force vector on suspended element, N

g	acceleration due to gravity ($1g \approx 9.81$ m/sec^2), m/sec^2
h	suspension height (suspended-element centroid to top plane of coils), m
$\mathbf{I}$	coil current vector, A
I_c	suspended-element transverse moment of inertia, kg-m^2
i	imaginary number
$\mathbf{KF}$	coefficient matrix of field gradient components
$\mathbf{KT}$	coefficient matrix of field components
K_{zn}	constant representing magnitude of B_{zn} produced by $I_{\max}$
$\mathbf{M}$	magnetization vector, A/m
m_c	suspended-element mass, kg
$\mathbf{T}$	total torque vector on suspended element, N-m
$\mathbf{T}_c$	magnetic torque vector on suspended element, N-m
$\mathbf{T}_d$	disturbance torque vector on suspended element, N-m
$\mathbf{T}_E$	suspended-element rate to Euler rate transformation matrix for a $3, 2, 1$ (z, y, x, respectively) rotation sequence
$\mathbf{T}_m$	inertial coordinate to suspended-element coordinate vector-transformation matrix
$\mathbf{V}$	velocity vector, m/sec
v	permanent magnet core volume, m^3
$\mathbf{W}_1$	weighting matrix (eq. (37))
$\mathbf{W}_2$	modified weighting matrix (eq. (41))
$\mathbf{X}$	state vector for linearized model
$\widetilde{\mathbf{X}}$	truncated state vector for linearized model
x, y, z	coordinates in orthogonal axis system, m
δ	small increment
θ	Euler orientation for $3, 2, 1$ rotation sequence, rad
$\mathbf{\Omega}$	angular velocity vector
∇	gradient operator

Subscripts:

b	electromagnet axes
ij	partial derivative of i component in j-direction
$(ij)k$	partial derivative of ij partial derivative in k-direction
max	maximum value
o	equilibrium condition
x, y, z	components along x-, y-, z-axes, respectively

1–8	coil numbers

Matrix notations:

$[\ ]$	matrix
$[\ ]^{-1}$	inverse of matrix
$\{\ \}$	column vector
$\{\ \}^T$	transpose of column vector
$\lfloor\ \rfloor$	row vector
$\lfloor\ \rfloor^T$	transpose of row vector

Dots over symbols denote derivatives with respect to time; a bar over a symbol indicates that it is referenced to suspended-element coordinates.

Simplified Analytical Model

This section presents a simplified analytical model of an LGMSS that is based on the model developed in reference 2. Extensions of the model developed in reference 2 include the addition of terms related to the change in field and field gradients with respect to suspended-element displacements. The equations are simplified by using small-angle assumptions and neglecting second-order terms involving suspended-element motion. The suspended element is a cylinder that contains a core composed of permanent magnet material assumed to be uniformly magnetized along the long axis. The suspended element is levitated over a planar array of electromagnets mounted in a circular configuration. Figure 1 is a schematic representation of a five-coil system that shows the coordinate systems and initial alignment. The suspended-element coordinate system consists of a set of orthogonal $\overline{x}$, $\overline{y}$, $\overline{z}$ body-fixed axes that define the motion of the suspended element with respect to inertial space. The suspended-element coordinate system is initially aligned with an orthogonal x, y, z system fixed in inertial space. A set of orthogonal x_b-, y_b-, z_b-axes, also fixed in inertial space, define the location of the electromagnet array with respect to the x, y, z system. The x_b- and y_b-axes are parallel to the x- and y-axes, respectively, and the z_b- and z-axes are aligned. The centers of the two axis systems are separated by the distance h.

Equations of Motion

The angular acceleration of the suspended element $\{\dot{\overline{\Omega}}\}$ in suspended-element coordinates can be written as (see ref. 2)

$$\left\{\dot{\overline{\Omega}}\right\} = \left(\frac{1}{I_c}\right)\{\overline{\mathbf{T}}\} \tag{1}$$

where I_c is the suspended-element moment of inertia about the axes of symmetry (y and z), and $\{\overline{\mathbf{T}}\}$ denotes the total torques on the suspended element ($T_{\overline{x}} = 0$). Since no torques occur about the x-axis, $\dot{\Omega}_{\overline{x}}$ is assumed to be 0 (see ref. 2) and is not included in equation (1). A bar over a variable indicates that it is referenced to suspended-element coordinates and $\{\ \}$ denotes a vector quantity. The torque $\{\overline{\mathbf{T}}\}$ can be expanded as

$$\{\overline{\mathbf{T}}\} = \{\overline{\mathbf{T}}_c\} + \{\overline{\mathbf{T}}_d\} \tag{2}$$

where $\{\overline{\mathbf{T}}_c\}$ denotes the control torques on the suspended element produced by the electromagnets and $\{\overline{\mathbf{T}}_d\}$ denotes external disturbance torques. The angular rates of the suspended element are obtained by integrating equation (1). The suspended-element Euler rates can be written as

$$\left\{\dot{\theta}\right\} = [\mathbf{T}_E]\left\{\overline{\Omega}\right\} \tag{3}$$

where $\mathbf{T}_E$ is the suspended-element rate to Euler rate transformation matrix for a 3, 2, 1 (that is, z, y, x) rotation sequence. By using small-angle and rate assumptions, equation (3) reduces to

$$\left\{\dot{\theta}\right\} \cong \left\{\overline{\boldsymbol{\Omega}}\right\} \tag{4}$$

where

$$\left\{\dot{\theta}\right\}^T = \lfloor\, \dot{\theta}_x \quad \dot{\theta}_y \quad \dot{\theta}_z \,\rfloor \tag{5}$$

The translational acceleration of the suspended element $\{\dot{\overline{\mathbf{V}}}\}$ in suspended-element coordinates can be written as

$$\left\{\dot{\overline{\mathbf{V}}}\right\} = (1/m_c)\left\{\overline{\mathbf{F}}\right\} \tag{6}$$

where m_c is the mass of the suspended element and $\{\overline{\mathbf{F}}\}$ denotes the total forces on the suspended element. The force $\{\overline{\mathbf{F}}\}$ can be expanded as

$$\left\{\overline{\mathbf{F}}\right\} = \left\{\overline{\mathbf{F}}_c\right\} + \left\{\overline{\mathbf{F}}_d\right\} + \left\{\overline{\mathbf{F}}_g\right\} \tag{7}$$

where $\{\overline{\mathbf{F}}_c\}$ denotes control forces on the suspended element produced by the electromagnets, $\{\overline{\mathbf{F}}_d\}$ denotes external disturbance forces, and $\{\overline{\mathbf{F}}_g\}$ consists of the force acting on the suspended element, due to gravity, transformed into suspended-element coordinates. The suspended-element translational rates are obtained by integrating equation (6). The suspended-element translational rates $\{\overline{\mathbf{V}}\}$ in inertial coordinates are given as

$$\{\mathbf{V}\} = [\mathbf{T}_m]^{-1}\left\{\overline{\mathbf{V}}\right\} \tag{8}$$

where $[\mathbf{T}_m]$ is the inertial coordinate to suspended-element coordinate vector-transformation matrix. By using small-angle and rate assumptions, equation (8) reduces to

$$\{\mathbf{V}\} \cong \left\{\overline{\mathbf{V}}\right\} \tag{9}$$

where

$$\{\mathbf{V}\}^T = \lfloor\, \dot{x} \quad \dot{y} \quad \dot{z} \,\rfloor \tag{10}$$

Magnetic Torques and Forces

The torque on the suspended element in a given orthogonal coordinate system can be approximated as

$$\{\mathbf{T}_c\} = v\,(\{\mathbf{M}\} \times \{\mathbf{B}\}) \tag{11}$$

where v is the volume of the permanent magnet core, $\{\mathbf{M}\}$ is the magnetization of the permanent magnet core, and $\{\mathbf{B}\}$ is the flux density at the centroid of the permanent magnet core produced by the electromagnets. (See ref. 2.) In suspended-element coordinates, the torque becomes

$$\left\{\overline{\mathbf{T}}_c\right\} = v\left(\left\{\overline{\mathbf{M}}\right\} \times [\mathbf{T}_m]\,\{\mathbf{B}\}\right) \tag{12}$$

Since, as mentioned earlier, the permanent magnet core is assumed to be uniformly magnetized along the $\overline{x}$-axis (long axis), $\{\overline{\mathbf{M}}\}$ becomes

$$\left\{\overline{\mathbf{M}}\right\}^T = \lfloor\, \mathbf{M}_{\overline{\mathbf{x}}} \quad 0 \quad 0 \,\rfloor \tag{13}$$

Similarly, the force on the suspended element can be approximated as

$$\{\mathbf{F_c}\} = v\,(\{\mathbf{M}\} \cdot \nabla)\,\{\mathbf{B}\} \tag{14}$$

where ∇ is the gradient operator (ref. 2). Taking the dot product and rearranging terms results in

$$\{\mathbf{F}_c\} = v\,[\partial\mathbf{B}]\,\{\mathbf{M}\} \tag{15}$$

where $[\partial\mathbf{B}]$ is a matrix of the gradients of $\mathbf{B}$. (See ref. 2.) By using the simplified notation $f_{ij} = \partial f_i/\partial j$, $[\partial\mathbf{B}]$ can be written as

$$[\partial\mathbf{B}] = \begin{bmatrix} B_{xx} & B_{xy} & B_{xz} \\ B_{yx} & B_{yy} & B_{yz} \\ B_{zx} & B_{zy} & B_{zz} \end{bmatrix} \tag{16}$$

In the region of the core, from Maxwell's equations, $\nabla \times \mathbf{B} = 0$ which results in $B_{ij} = B_{ji}$. In suspended-element coordinates, the force becomes

$$\{\overline{\mathbf{F}}_c\} = v\,[\mathbf{T}_m]\,[\partial\mathbf{B}]\,[\mathbf{T}_m]^{-1}\,\{\overline{\mathbf{M}}\} \tag{17}$$

By using small-angle assumptions, the relationship $B_{ij} = B_{ji}$, and assuming that $\theta_x = 0$ (ref. 2), the torque and force equations reduce to

$$T_{c\bar{y}} = vM_{\bar{x}}\left(-\theta_y B_x - B_z\right) \tag{18}$$

$$T_{c\bar{z}} = vM_{\bar{x}}\left(-\theta_z B_x + B_y\right) \tag{19}$$

$$F_{c\bar{x}} = vM_{\bar{x}}\left(B_{xx} + 2\theta_z B_{xy} - 2\theta_y B_{xz}\right) \tag{20}$$

$$F_{c\bar{y}} = vM_{\bar{x}}\left(-\theta_z B_{xx} + B_{xy} + \theta_z B_{yy} - \theta_y B_{yz}\right) \tag{21}$$

$$F_{c\bar{z}} = vM_{\bar{x}}\left(\theta_y B_{xx} + B_{xz} + \theta_z B_{yz} - \theta_y B_{zz}\right) \tag{22}$$

The torques and forces are functions of rotations and translations about the nominal operating point and coil currents $(I_1, I_2, \ldots, I_n)$; thus,

$$\left\{ \begin{array}{c} \overline{\mathbf{T}}_c \\ \hline \overline{\mathbf{F}}_c \end{array} \right\} = f\left(\lfloor\, \theta_y \quad \theta_z \quad x \quad y \quad z \,\rfloor^T, \lfloor\, I_1 \quad I_2 \quad \ldots \quad I_n \,\rfloor^T\right) \tag{23}$$

Disturbance Torques and Forces

The only significant disturbance acting on the suspended element is along the z-axis and is equal to its weight

$$\{\mathbf{F}_g\}^T = \lfloor\, 0 \quad 0 \quad -m_c g \,\rfloor \tag{24}$$

where g is the acceleration due to gravity. Other disturbance torques and forces are ignored. Transforming to suspended-element coordinates gives

$$\{\overline{\mathbf{F}}_g\} = [\mathbf{T}_m]\,\{\mathbf{F}_g\} \tag{25}$$

Performing the transformation under the assumptions made for equations (18)–(22) results in

$$F_{g\bar{x}} = \theta_y\,(m_c g) \tag{26}$$

$$F_{g\bar{y}} = 0 \tag{27}$$

$$F_{g\bar{z}} = -m_c g \tag{28}$$

Linearized Equations

The equations of motion are in the form

$$\left\{\dot{\mathbf{X}}\right\} = f\left(\left\{\begin{array}{c}\overline{\mathbf{T}}/I_c \\ \overline{\mathbf{F}}/m_c\end{array}\right\}\right) \tag{29}$$

where

$$\{\mathbf{X}\}^T = \lfloor\, \Omega_{\bar{y}} \quad \Omega_{\bar{z}} \quad \theta_y \quad \theta_z \quad V_{\bar{x}} \quad V_{\bar{y}} \quad V_{\bar{z}} \quad x \quad y \quad z \,\rfloor \tag{30}$$

The only nonzero disturbance acting on the suspended element is assumed to be $\{\mathbf{F}_g\}$. (See eq. (24).) From the previous equations,

$$\left\{\begin{array}{c}\overline{\mathbf{T}}/I_c \\ \overline{\mathbf{F}}/m_c\end{array}\right\} = f\left(\tilde{\mathbf{X}}, \mathbf{I}\right) \tag{31}$$

where

$$\left\{\tilde{\mathbf{X}}\right\}^T = \lfloor\, \theta_y \quad \theta_z \quad x \quad y \quad z \,\rfloor \tag{32}$$

and

$$\{\mathbf{I}\}^T = \lfloor\, I_1 \quad I_2 \quad \ldots \quad I_n \,\rfloor \tag{33}$$

The equations can be linearized around the nominal operating point $\mathbf{X}_o$, $\mathbf{I}_o$ by performing a Taylor series expansion. Neglecting second-order terms and subtracting out $\mathbf{X}_o$ results in

$$\left\{\delta\dot{\mathbf{X}}\right\} = [\mathcal{A}]\{\delta\mathbf{X}\} + [\mathcal{B}]\{\delta\mathbf{I}\} \tag{34}$$

where

$$\mathcal{A} = \mathbf{W}_1\, \partial f\left(\left\{\begin{array}{c}\overline{\mathbf{T}} \\ \overline{\mathbf{F}}\end{array}\right\}\right) \Big/ \partial\mathbf{X}\Big|_{\mathbf{X}_o,\mathbf{I}_o} \tag{35}$$

$$\mathcal{B} = \mathbf{W}_1\, \partial f\left(\left\{\begin{array}{c}\overline{\mathbf{T}} \\ \overline{\mathbf{F}}\end{array}\right\}\right) \Big/ \partial\mathbf{I}\Big|_{\mathbf{X}_o,\mathbf{I}_o} \tag{36}$$

and

$$\mathbf{W}_1 = \begin{bmatrix} 1/I_c & 0 & 0 & 0 & 0 & 0 & 0 & 0 & 0 & 0 \\ 0 & 1/I_c & 0 & 0 & 0 & 0 & 0 & 0 & 0 & 0 \\ 0 & 0 & 1 & 0 & 0 & 0 & 0 & 0 & 0 & 0 \\ 0 & 0 & 0 & 1 & 0 & 0 & 0 & 0 & 0 & 0 \\ 0 & 0 & 0 & 0 & 1/m_c & 0 & 0 & 0 & 0 & 0 \\ 0 & 0 & 0 & 0 & 0 & 1/m_c & 0 & 0 & 0 & 0 \\ 0 & 0 & 0 & 0 & 0 & 0 & 1/m_c & 0 & 0 & 0 \\ 0 & 0 & 0 & 0 & 0 & 0 & 0 & 1 & 0 & 0 \\ 0 & 0 & 0 & 0 & 0 & 0 & 0 & 0 & 1 & 0 \\ 0 & 0 & 0 & 0 & 0 & 0 & 0 & 0 & 0 & 1 \end{bmatrix} \tag{37}$$

Expanding $\mathcal{A}$ results in

$$\mathcal{A} = \mathbf{W}_1 \begin{bmatrix} \partial T_{\overline{y}}/\partial \Omega_{\overline{y}} & \partial T_{\overline{y}}/\partial \Omega_{\overline{z}} & \partial T_{\overline{y}}/\partial \theta_y & \cdots & \partial T_{\overline{y}}/\partial z \\ \partial T_{\overline{z}}/\partial \Omega_{\overline{y}} & \partial T_{\overline{z}}/\partial \Omega_{\overline{z}} & \cdots & & \vdots \\ \partial \Omega_{\overline{y}}/\partial \Omega_{\overline{y}} & \cdots & & & \\ \vdots & & & & \\ \partial V_{\overline{z}}/\partial \Omega_{\overline{y}} & \cdots & & & \partial V_{\overline{z}}/\partial z \end{bmatrix} \tag{38}$$

which reduces to

$$\mathcal{A} = \mathbf{W}_1 \begin{bmatrix} 0 & 0 & T_{\overline{y}\theta_y} & T_{\overline{y}\theta_z} & 0 & 0 & 0 & T_{\overline{y}x} & T_{\overline{y}y} & T_{\overline{y}z} \\ 0 & 0 & T_{\overline{z}\theta_y} & T_{\overline{z}\theta_z} & 0 & 0 & 0 & T_{\overline{z}x} & T_{\overline{z}y} & T_{\overline{z}z} \\ 1 & 0 & 0 & 0 & 0 & 0 & 0 & 0 & 0 & 0 \\ 0 & 1 & 0 & 0 & 0 & 0 & 0 & 0 & 0 & 0 \\ 0 & 0 & F_{\overline{x}\theta_y} & F_{\overline{x}\theta_z} & 0 & 0 & 0 & F_{\overline{x}x} & F_{\overline{x}y} & F_{\overline{x}z} \\ 0 & 0 & F_{\overline{y}\theta_y} & F_{\overline{y}\theta_z} & 0 & 0 & 0 & F_{\overline{y}x} & F_{\overline{y}y} & F_{\overline{y}z} \\ 0 & 0 & F_{\overline{z}\theta_y} & F_{\overline{z}\theta_z} & 0 & 0 & 0 & F_{\overline{z}x} & F_{\overline{z}y} & F_{\overline{z}z} \\ 0 & 0 & 0 & 0 & 1 & 0 & 0 & 0 & 0 & 0 \\ 0 & 0 & 0 & 0 & 0 & 1 & 0 & 0 & 0 & 0 \\ 0 & 0 & 0 & 0 & 0 & 0 & 1 & 0 & 0 & 0 \end{bmatrix} \tag{39}$$

Finally, by using the expressions for torques and forces developed earlier (eqs. (18)–(22) and (26)–(28)), $\mathcal{A}$ becomes

$$\mathcal{A} = \mathbf{W}_2 \begin{bmatrix} 0 & 0 & -B_x & 0 & 0 & 0 & 0 & -B_{xz} & -B_{yz} & -B_{zz} \\ 0 & 0 & 0 & -B_x & 0 & 0 & 0 & B_{xy} & B_{yy} & B_{yz} \\ 1 & 0 & 0 & 0 & 0 & 0 & 0 & 0 & 0 & 0 \\ 0 & 1 & 0 & 0 & 0 & 0 & 0 & 0 & 0 & 0 \\ 0 & 0 & \left(\frac{m_c g}{v M_{\overline{x}}} - 2B_{xz}\right) & 2B_{xy} & 0 & 0 & 0 & B_{(xx)x} & B_{(xx)y} & B_{(xx)z} \\ 0 & 0 & B_{yz} & (B_{yy} - B_{xx}) & 0 & 0 & 0 & B_{(xy)x} & B_{(xy)y} & B_{(xy)z} \\ 0 & 0 & (B_{xx} - B_{zz}) & B_{yz} & 0 & 0 & 0 & B_{(xz)x} & B_{(xz)y} & B_{(xz)z} \\ 0 & 0 & 0 & 0 & 1 & 0 & 0 & 0 & 0 & 0 \\ 0 & 0 & 0 & 0 & 0 & 1 & 0 & 0 & 0 & 0 \\ 0 & 0 & 0 & 0 & 0 & 0 & 1 & 0 & 0 & 0 \end{bmatrix} \tag{40}$$

where the notation $\partial f_{ij}/\partial k = f_{(ij)k}$ has been used and

$$\mathbf{W}_2 = \begin{bmatrix} vM_{\overline{x}}/I_c & 0 & 0 & 0 & 0 & 0 & 0 & 0 & 0 & 0 \\ 0 & vM_{\overline{x}}/I_c & 0 & 0 & 0 & 0 & 0 & 0 & 0 & 0 \\ 0 & 0 & 1 & 0 & 0 & 0 & 0 & 0 & 0 & 0 \\ 0 & 0 & 0 & 1 & 0 & 0 & 0 & 0 & 0 & 0 \\ 0 & 0 & 0 & 0 & vM_{\overline{x}}/m_c & 0 & 0 & 0 & 0 & 0 \\ 0 & 0 & 0 & 0 & 0 & vM_{\overline{x}}/m_c & 0 & 0 & 0 & 0 \\ 0 & 0 & 0 & 0 & 0 & 0 & vM_{\overline{x}}/M_c & 0 & 0 & 0 \\ 0 & 0 & 0 & 0 & 0 & 0 & 0 & 1 & 0 & 0 \\ 0 & 0 & 0 & 0 & 0 & 0 & 0 & 0 & 1 & 0 \\ 0 & 0 & 0 & 0 & 0 & 0 & 0 & 0 & 0 & 1 \end{bmatrix} \tag{41}$$

Next, expanding $\mathcal{B}$ results in

$$\mathcal{B} = \mathbf{W}_1 \begin{bmatrix} \partial T_{\overline{y}}/\partial I_1 & \partial T_{\overline{y}}/\partial I_2 & \cdots & \partial T_{\overline{y}}/\partial I_n \\ \partial T_{\overline{z}}/\partial I_1 & \partial T_{\overline{z}}/\partial I_2 & \cdots & \\ \partial \Omega_{\overline{y}}/\partial I_1 & \cdots & & \\ \vdots & & & \\ \partial V_{\overline{z}}/\partial I_1 & & & \end{bmatrix} \tag{42}$$

Expanding the first term in equation (42) gives

$$\partial T_{\overline{y}}/\partial I_1 = vM_{\overline{x}} \left[-\theta_y \left(\partial B_x/\partial I_1 \right) - \left(\partial B_z/\partial I_1 \right) \right] \tag{43}$$

Because θ_y is small, the term $\theta_y(\partial B_x/\partial I_1)$ is neglected. Since the fields and gradients are linear functions of coil currents, the components of B_z produced by coil n of an n-coil system can be written as

$$B_{zn} = K_{zn} \left(I_n / I_{\max} \right) \tag{44}$$

where $I_{\max}$ is the maximum coil current, K_{zn} is a constant that represents the magnitude of B_{zn} produced by $I_{\max}$, and I_n is the coil current. For the total system, B_z can be written as

$$B_z = \left(1/I_{\max} \right) \lfloor \mathbf{K}_z \rfloor \{ \mathbf{I} \} \tag{45}$$

where

$$\lfloor \mathbf{K}_z \rfloor = \lfloor \, K_{z1} \quad K_{z2} \quad \ldots \quad K_{zn} \, \rfloor \tag{46}$$

and

$$\{ \mathbf{I} \}^T = \lfloor \, I_1 \quad I_2 \quad \ldots \quad I_n \, \rfloor \tag{47}$$

(See ref. 2.) Since the elements of $\lfloor \mathbf{K}_z \rfloor$ are constants

$$\partial B_z / \partial \mathbf{I} = \left(1/I_{\max} \right) \lfloor \mathbf{K}_z \rfloor \tag{48}$$

Similar results are obtained for the other fields and gradients. Terms in $\mathcal{B}$ related to the identities $\dot{\theta}_y = \Omega_{\overline{y}}, \dot{\theta}_z = \Omega_{\overline{z}}, \dot{x} = V_{\overline{x}}, \dot{y} = V_{\overline{y}}$, and $\dot{z} = V_{\overline{z}}$ are 0. Then, $\mathcal{B}$ becomes

$$\mathcal{B} = (1/I_{\max})\,\mathbf{W}_2 \begin{bmatrix} -\lfloor \mathbf{K}_z \rfloor \\ \lfloor \mathbf{K}_y \rfloor \\ \lfloor 0 \rfloor \\ \lfloor 0 \rfloor \\ \lfloor \mathbf{K}_{xx} \rfloor \\ \lfloor \mathbf{K}_{xy} \rfloor \\ \lfloor \mathbf{K}_{xz} \rfloor \\ \lfloor 0 \rfloor \\ \lfloor 0 \rfloor \\ \lfloor 0 \rfloor \end{bmatrix} \tag{49}$$

Initial Conditions

The suspended element is assumed to be initially suspended in equilibrium at a distance h above the electromagnet array with the suspended-element coordinates initially aligned with the inertial coordinates as shown in figure 1. In equilibrium, $F_{\overline{x}} = F_{\overline{y}} = 0$ and the only force on the suspended element is along the $\overline{z}$-axis and is equal to the suspended-element weight

$$F_{\overline{z}} = m_c g \tag{50}$$

From equations (18)-(22), we have

$$B_y = B_z = B_{xx} = B_{xy} = 0 \tag{51}$$

and

$$B_{xz} = \frac{m_c g}{v M_{\overline{x}}} \tag{52}$$

In equilibrium, by using the relationship of equation (52), element (5,3) of the matrix in equation (40) reduces to

$$\frac{m_c g}{v M_{\overline{x}}} - 2B_{xz} = -B_{xz} \tag{53}$$

From equation (45), the controlled fields and gradients as a function of $\mathbf{I}_o$ can be written as

$$(1/I_{\max}) \begin{bmatrix} \lfloor \mathbf{K}_y \rfloor \\ \lfloor \mathbf{K}_z \rfloor \\ \lfloor \mathbf{K}_{xx} \rfloor \\ \lfloor \mathbf{K}_{xy} \rfloor \\ \lfloor \mathbf{K}_{xz} \rfloor \end{bmatrix} \{\mathbf{I}_o\} = \lfloor\, B_y \quad B_z \quad B_{xx} \quad B_{xy} \quad B_{xz} \,\rfloor^T \tag{54}$$

For a five-coil system, $\{\mathbf{I}_o\}$ can be found by direct inversion of the $\mathbf{K}$ matrix in equation (54). The generalized inverse (ref. 4) is used to calculate $\{\mathbf{I}_o\}$ for higher order coil systems. This produces a solution where the 2-norm of the current vector $\{\mathbf{I}_o\}$ is minimized (i.e., minimum $\Sigma \mathbf{I}^2$). If all electromagnets are the same size and have the same characteristics, the resistive power is minimized for room-temperature electromagnets and the stored energy is minimized in all cases. Note that if the electromagnets are of varying sizes, scaling of the columns of the $\mathbf{K}$ matrix may be necessary.

Alternative solutions can be found if different constraints are applied. The solution giving the minimum ∞-norm of the current vector corresponds to the maximum individual current

value being minimized. With fixed core magnetization, this also gives the current distribution required for maximum force and moment capability. However, this solution has been found to often exhibit discontinuities with varying suspended-element orientation (ref. 5) and was, therefore, not addressed in this paper. Once $\{\mathbf{I}_o\}$ is determined, the uncontrolled fields and gradients required to complete the $\mathcal{A}$ matrix can be calculated.

One of the objectives of LGMSS development is to allow positioning of the suspended element through large angles in yaw (θ_z) up to 360° (ref. 3). As the suspended element is rotated, the equilibrium suspension currents will change. In the appendix of reference 2, the equilibrium currents are developed as a function of yaw angle and initial torques and forces on the suspended element. Rearranging equation (A12) in reference 2 results in

$$(1/I_{\max}) \begin{bmatrix} [\mathbf{KT}] \\ --- \\ [\mathbf{KF}] \end{bmatrix} \{\mathbf{I}_o\} = \lfloor\, B_z \quad B_y \quad B_{xx} \quad B_{xy} \quad B_{xz} \,\rfloor^T \tag{55}$$

where

$$\lfloor\, B_z \quad B_y \quad B_{xx} \quad B_{xy} \quad B_{xz} \,\rfloor^T = (1/vM_{\overline{x}}) \begin{Bmatrix} \overline{\mathbf{T}} \\ \overline{\mathbf{F}} \end{Bmatrix} \tag{56}$$

By rearranging $[\mathbf{KT}]$, equation (48) can be written as

$$(1/I_{\max}) \begin{bmatrix} -\sin\theta_z \lfloor \mathbf{K}_x \rfloor + \cos\theta_z \lfloor \mathbf{K}_y \rfloor \\ \lfloor \mathbf{K}_z \rfloor \\ ---------- \\ [\mathbf{KF}] \end{bmatrix} \{\mathbf{I}_o\} = \lfloor\, B_y \quad B_z \quad B_{xx} \quad B_{xy} \quad B_{xz} \,\rfloor^T \tag{57}$$

where

$$[\mathbf{KF}] = \begin{bmatrix} \cos^2\theta_z \lfloor \mathbf{K}_{xx} \rfloor + 2\cos\theta_z \sin\theta_z \lfloor \mathbf{K}_{xy} \rfloor + \sin^2\theta_z \lfloor \mathbf{K}_{yy} \rfloor \\ -\cos\theta_z \sin\theta_z \lfloor \mathbf{K}_{xx} \rfloor + (\cos^2\theta_z - \sin^2\theta_z) \lfloor \mathbf{K}_{xy} \rfloor + \cos\theta_z \sin\theta_z \lfloor \mathbf{K}_{yy} \rfloor \\ \cos\theta_z \lfloor \mathbf{K}_{xz} \rfloor + \sin\theta_z \lfloor \mathbf{K}_{yz} \rfloor \end{bmatrix} \tag{58}$$

Results and Discussion

In order to evaluate the open-loop behavior of the LGMSS, the eigenvalues and corresponding eigenvectors of the $\mathcal{A}$ matrix of equation (34) were calculated for each coil configuration. The eigenvalues represent the frequencies of the open-loop modes of the system, and the eigenvectors represent the mode shapes (ref. 6). The system was found to be controllable from coil currents and observable from suspended-element positions for each coil configuration.

Five-Coil Configuration

The value of B_{xz} required for suspension is found to be 0.096 T/m from using equation (52) with the parameters given in the appendix. In principle, with the correct coil configuration and current distribution, this can be the only electromagnet field or field gradient present. Therefore, substituting this value into equation (40) (with all other field and gradient values equal to 0) should allow the fundamental modes of the system to be determined. Making the substitution and calculating the eigenvalues and corresponding eigenvectors results in the values presented in table 1. From the table it can be seen that two fundamental modes occur and both involve motion along the x-axis and rotation about the y-axis. Physically, they result from two interactions between the displaced suspended element and the B_{xz} gradient. Mode 1, which is

an unstable mode, is related to the $T_{\bar{y}x}$ term in equation (39). This term initiates a negative rotation (pitch) after an x-displacement. Mode 2, which is a stable oscillatory mode, is related to the $F_{\bar{x}\theta_y}$ term in equation (39). This term initiates a negative x-displacement following a pitching rotation. The mode shapes are shown in figure 2. For convenience, mode 1 is referred to as a *tumbling* mode and mode 2 is referred to as a *rocking* mode.

With the value of B_{xz} given previously, the currents required to provide equilibrium suspension for the five-coil configuration were found to be

$$\{\mathbf{I}_o/I_{\max}\}^T = \lfloor -0.7751 \quad -0.2398 \quad 0.6274 \quad 0.6274 \quad -0.2398 \rfloor \tag{59}$$

by using equation (54). These currents were then used to calculate the remaining fields and gradients required to determine the elements of equation (40). The results are presented in table 2. Note that some values are 0 through symmetry about the xz-plane, some are nominally 0 by choice of electromagnet currents, and others are found to be approximately 0 for this particular configuration.

Under the assumptions of reference 3, the dominant term in the open-loop equations was B_x. Adding the value of B_x from table 2 to equation (40) and calculating the eigenvalues and corresponding eigenvectors results in the values presented in table 3. The frequencies of modes 1 and 2 from table 1 have been substantially modified by introducing B_x, with the result that another mode has been added. Mode 3 is an unstable rotational mode about the z-axis and is caused by the magnetization vector trying to align itself with the applied field (the *compass-needle* effect). Mode 1 represents a combination of this effect and the tumbling motion due to B_{xz}. For convenience, modes 1 and 3 will now be referred to as *compass-needle* modes. With only B_x present, the frequencies of both compass-needle modes become 12.862 rad/sec, and mode 2 is absent. This matches the results in reference 3 and is consistent with the simplifying assumptions made therein. The eigenvalues and corresponding eigenvectors of equation (40), from using the remaining values in table 2, are presented in table 4. From table 4 the number of modes is seen to increase to 5. Mode 5 is a translational divergence in the y-direction because of the $F_{\bar{y}y}$ term in equation (39). Mode 4 is a stable oscillatory mode in the z-direction because of the $F_{\bar{z}z}$ term in equation (39). The frequency of mode 1, which is the highest frequency mode, is increased by a small amount, the frequency of mode 2 is decreased, and the frequency of mode 3 is unchanged. The mode shapes are shown in figure 2.

A review of the results presented in tables 1, 3, and 4 shows that the highest frequency modes are compass-needle modes caused by the presence of B_x. The highest frequency of the open-loop modes is critical because of the existence of controller time delays, large electromagnet time constants, limited frequency response of power supplies, and practical constraints on position sensor sample rate. Adding second-order gradient terms to the system model increases the number of open-loop modes. However, the additional modes have much lower frequencies and do not modify the high-frequency compass-needle terms significantly. Since the highest frequency modes are caused by the presence of B_x and since B_x is uncontrolled (see eq. (49)) with the five-coil system, a decision was made to investigate the control of B_x (and therefore the highest open-loop frequencies) by increasing the number of coils. The results are presented in later sections.

The equilibrium suspension current can be determined as a function of yaw orientation by using equation (57). The results presented in figure 3 show that the variation of current in each coil is sinusoidal. Further, since all the coefficients in $\lfloor \mathbf{K}_z \rfloor$ are identical because of the axial symmetry of the coil configuration, row 2 of equation (57) implies that $\sum_{n=1}^{5} I_n = 0$. This is also

true for all other coil configurations investigated herein. The open-loop modes do not change significantly as a function of yaw orientation.

Six-Coil Configuration

The currents required to provide equilibrium suspension for the six-coil configuration (by using eq. (54) and the value of B_{xz} given previously) were found to be

$$\{\mathbf{I}_o/I_{\max}\}^T = \lfloor -0.7973 \quad -0.3947 \quad 0.3947 \quad 0.7973 \quad 0.3947 \quad -0.3947 \rfloor \tag{60}$$

These currents were then used to calculate the remaining fields and gradients required to determine the elements of equation (40). The results are presented in table 5. The eigenvalues and corresponding eigenvectors of equation (40), by using the values from table 5, are presented in table 6. The results are essentially the same as for the five-coil configuration.

To investigate the control of B_x, as discussed previously, K_x and B_x were added to equation (54). Setting B_x to 0 and solving for the currents results in

$$\{\mathbf{I}_o/I_{\max}\}^T = \lfloor -239.9959 \quad 241.1959 \quad -241.1959 \quad 239.9959 \quad -241.1959 \quad 241.1959 \rfloor \tag{61}$$

This solution is obviously unacceptable because the magnitudes of the currents are all very large. Also, the coils are driven in a $+/-/+/-$ sequence which indicates that the field at the suspended element is the sum of opposing and nearly cancelling contributions from all coils. This implies that independent control of B_x and B_{xz} is not a viable approach with this configuration.

The variation of equilibrium coil currents as a function of yaw orientation, using the generalized inverse to solve equation (57), is shown in figure 4. Again, the modes of the system do not change significantly as a function of yaw orientation.

Seven-Coil Configuration

The currents required to provide equilibrium suspension for the seven-coil configuration (by using eq. (54) and the value of B_{xz} given previously) were found to be

$$\{\mathbf{I}_o/I_{\max}\}^T = \lfloor -0.8688 \quad -0.5365 \quad 0.1897 \quad 0.7812 \quad 0.7812 \quad 0.1897 \quad -0.5365 \rfloor \tag{62}$$

These currents were then used to calculate the remaining fields and gradients required to determine the elements of equation (40). The results are presented in table 7. The eigenvalues and corresponding eigenvectors of equation (40), by using the values from table 7, are presented in table 8. The results are essentially the same as for the other configurations.

Solving for the currents required to set B_x to 0 as described previously results in

$$\{\mathbf{I}_o/I_{\max}\}^T = \lfloor -132.6562 \quad 119.2667 \quad -82.8908 \quad 29.9521 \quad 29.9521 \quad -82.8908 \quad 119.2667 \rfloor \tag{63}$$

This solution is also unacceptable because of the high currents required. Again, the coils are driven approximately in a $+/-/+/-$ sequence. (Coils 4 and 5 behave as a single coil.)

The variation of equilibrium coil currents as a function of yaw orientation is shown in figure 5. The modes of the system do not change significantly as a function of yaw orientation.

Eight-Coil Configuration

The currents required to provide equilibrium suspension for the eight-coil configuration were found to be

$$\{\mathbf{I}_o/I_{\max}\}^T = \lfloor -0.9753 \quad -0.6843 \quad 0 \quad 0.6843 \quad 0.9753 \quad 0.6843 \quad 0 \quad -0.6843 \rfloor \tag{64}$$

These currents were then used to calculate the remaining fields and gradients required to determine the elements of equation (40). The results are presented in table 9. The eigenvalues and corresponding eigenvectors of equation (40), by using the values from table 9, are presented in table 10. The results are essentially the same as for the other configurations.

Again, solving for the currents required to set B_x to 0 results in

$$\{\mathbf{I}_o/I_{\max}\}^T = \lfloor -204.016 \quad 144.012 \quad 0 \quad -144.012 \quad 204.016 \quad -144.012 \quad 0 \quad 144.012 \rfloor \tag{65}$$

These currents are similar in magnitude to the currents required by the previous configurations, and again the coils are driven approximately in a $+/-/+/-$ sequence. (Coils 3 and 7 have zero current.)

The variation of equilibrium coil currents as a function of yaw orientation is shown in figure 6. The modes of the system do not change significantly as a function of yaw orientation.

Concluding Remarks

The open-loop characteristics of a Large-Gap Magnetic Suspension System (LGMSS) have been investigated and numerical results are presented. The system was found to be controllable from coil currents and observable from suspended-element positions for all coil configurations examined. The basic system investigated provides five-degree-of-freedom control of a suspended element which is a cylinder that contains a core composed of permanent magnet material. The magnetization vector of the permanent magnet core is horizontal (along the long axis of the cylinder). The magnetic actuators are air core electromagnets mounted in a planar array. The basic system uses five electromagnets since this is the minimum configuration for five-degree-of-freedom control.

The results indicate that the highest frequency open-loop modes are caused by the presence of an x-component of the field (B_x) which is required to produce equilibrium suspension of the suspended element. These modes are called compass-needle modes because they result from the magnetization vector trying to align itself with the applied field (the compass-needle effect). The highest frequency of the open-loop modes is critical because of practical constraints such as position-sensor sample rates. Previous analyses have used the simplifying assumption that the change in electromagnet field and field gradients with respect to suspended-element displacements is negligible. Adding these effects increased the number of open-loop modes from three to five. However, the additional modes have much lower frequencies and do not modify the high-frequency compass-needle modes significantly. The highest frequency modes, as discussed earlier, are caused by the presence of B_x. Since B_x is uncontrolled with the minimum five-coil configuration, it was thought that independent control of B_x (and thus the magnitude of the highest open-loop frequencies) would be possible by increasing the number of coils.

Configurations utilizing six, seven, and eight coils were investigated. The results indicated that independently controlling B_x requires very high coil currents because the solution for controlling B_x resulted in the coils being driven in a $+/-/+/-$ sequence. This indicates that the field at the suspended element is the sum of opposing and nearly cancelling contributions from all coils. The conclusion was made that independent control of B_x with a planar array of the type investigated and a permanent magnet core with a horizontal magnetization vector is not a viable approach. Increasing the number of coils had an insignificant effect on mode shapes and frequencies.

NASA Langley Research Center
Hampton, VA 23681-0001
August 18, 1992

Appendix

Electromagnet Fields and Gradients

This appendix presents, in the form of tables, the components of fields and gradients (including second-order gradients) generated by the electromagnets in configurations of five, six, seven, and eight coils mounted in planar arrays. It should be noted that the full set of components is not included in the tables since $B_{ij} = B_{ji}$ and $B_{(ij)k} = B_{(ik)j} = B_{(jk)i}$. The coils are arranged in a circular configuration and are constrained to fit inside an 8- by 8- by 4-ft volume. (See ref. 1.) An example of a five-coil configuration is shown in figure A1. Values of fields and gradients are calculated by using the program VF/GFUN (ref. 7), which is a finite-element code using integral equation formulation for the solution of the magnetization of iron regions. For the results shown in this report, only the pre- and post-processor OPERA was required. OPERA calculates the field from complicated conductor geometries through using numerical integration techniques. The parameters of the suspended element and core are the same as those in reference 8 and are presented in table A1.

Five-Coil Configuration

The electromagnet parameters for the baseline five-coil configuration are the same as those in reference 8 and are presented in table A2(a). Values of the fields and first-order gradient components are given in table A2(b), and second-order gradient components are given in table A2(c). A schematic representation of the five-coil configuration is presented in figure A1.

Six-Coil Configuration

An extra coil of the same size can be added to the baseline five-coil configuration without violating the volume constraint given previously. The parameters for this configuration are given in table A3(a). Values of the fields and first-order gradient components are given in table A3(b), and values of second-order gradient components are given in table A3(c). A schematic representation of the six-coil configuration is presented in figure A2.

Seven-Coil Configuration

To add a seventh coil without violating the volume constraint, the coil diameters must be reduced. In an attempt to preserve a natural progression of geometry, this reduction was done by holding the proportions of the coils and the maximum ampere turns fixed. This resulted in an increase in maximum current density. Parameters of the seven-coil configuration are given in table A4(a). Values of the field and first-order gradient components are given in table A4(b), and values of the second-order gradient components are given in table A4(c). A schematic representation of the seven-coil configuration is shown in figure A3.

Eight-Coil Configuration

Adding an eighth coil requires a further reduction in coil diameter, which was accomplished in the same manner as that used with the seven-coil configuration. Parameters for the eight-coil configuration are given in table A5(a). Values of the field and first-order gradient components are given in table A5(b), and values of the second-order gradient components are given in table A5(c). A schematic representation of the eight-coil configuration is presented in figure A4.

Table A1. Suspended-Element and Permanent Magnet Core Parameters

Core diameter, m	0.1016
Core length, m	0.3048
Suspended-element mass,[a] m_c, kg	23.11
Suspended-element inertia,[a] I_c, kg-m^2	0.6
Core volume, v, m^3	2.471×10^{-3}
Core magnetization, M_x, A/m	9.5493×10^{-5}
Suspended-element suspension height, h, m	0.9144

[a]Mass and inertia quoted include nonmagnetic components surrounding the core (ref. 8).

Table A2. Five-Coil Configuration

(a) Electromagnet parameters

Electromagnet outer radius, m	0.386
Electromagnet inner radius, m	0.173
Electromagnet height, m	0.493
Location radius,[a] m	0.7
Maximum current density, A/cm^2	1535.87

[a]Distance from center of array to axis of given coil.

(b) Electromagnet fields and first-order gradients

Electromagnet	B_x, T	B_y, T	B_z, T	B_{xx}, T/m	B_{xy}, T/m	B_{xz}, T/m	B_{yy}, T/m	B_{yz}, T/m	B_{zz}, T/m
1	0.0216	0	−0.0198	0.0092	0	−0.0497	−0.0306	0	0.0215
2	.0067	.0206	↓	−.0269	.0118	.0152	.0054	−.0472	↓
3	−.0175	.0127	↓	−.0046	−.0191	.0400	−.0170	−.0290	↓
4	−.0175	−.0127	↓	−.0046	.0191	.0400	−.0170	.0290	↓
5	.0067	−.0206	↓	−.0269	−.0118	−.0152	.0054	.0472	↓

(c) Electromagnet second-order gradients

Electromagnet	$B_{(xx)x}$, T/m/m	$B_{(xy)x}$, T/m/m	$B_{(xz)x}$, T/m/m	$B_{(xy)y}$, T/m/m	$B_{(xy)z}$, T/m/m	$B_{(xz)z}$, T/m/m
1	−0.0695	0	−0.0716	−0.0573	0	0.1276
2	−.0498	−.0452	.0570	.011	−.0416	.0394
3	.0848	.0058	−.0222	.0178	.0679	−.1032
4	.0848	−.0058	−.0222	.0178	−.0679	−.1032
5	−.0498	.0452	.0570	.011	.0416	.0394

Table A3. Six-Coil Configuration

(a) Electromagnet parameters

Electromagnet outer radius, m	0.386
Electromagnet inner radius, m	0.173
Electromagnet height, m	0.493
Location radius, m	0.822
Maximum current density, A/cm^2	1535.87

(b) Electromagnet fields and first-order gradients

Electromagnet	B_x, T	B_y, T	B_z, T	B_{xx}, T/m	B_{xy}, T/m	B_{xz}, T/m	B_{yy}, T/m	B_{yz}, T/m	B_{zz}, T/m
1	0.0201	0	−0.0143	0.0156	0	−0.0404	−0.0242	0	0.0087
2	.0100	.0174	↓	−.0143	.0173	−.0200	.0055	−.0349	↓
3	−.0100	.0174	↓	−.0143	−.0173	.0200	.0055	−.0349	↓
4	−.0201	0	↓	.0156	0	.0404	−.0242	0	↓
5	−.0100	−.0174	↓	−.0143	.0173	.0200	.0055	.0349	↓
6	.0100	−.0174	↓	−.0143	−.0173	−.0200	.0055	.0349	↓

(c) Electromagnet second-order gradients

Electromagnet	$B_{(xx)x}$, T/m/m	$B_{(xy)x}$, T/m/m	$B_{(xz)x}$, T/m/m	$B_{(xy)y}$, T/m/m	$B_{(xy)z}$, T/m/m	$B_{(xz)z}$, T/m/m
1	−0.0356	0	−0.0775	−0.0485	0	0.0839
2	−.0589	−.0183	.0175	.0171	−.0545	.0420
3	.0589	−.0183	.0175	−.0171	.0545	−.0420
4	.0356	0	−.0775	.0485	0	−.0839
5	.0589	.0183	.0175	−.0171	−.0545	−.0420
6	−.0589	.0183	.0175	.0171	.0545	.0420

Table A4. Seven-Coil Configuration

(a) Electromagnet parameters

Electromagnet outer radius, m	0.358
Electromagnet inner radius, m	0.160
Electromagnet height, m	0.457
Location radius, m	0.883
Maximum current density, A/cm^2	1785.5

(b) Electromagnet fields and first-order gradients

Electromagnet	B_x, T	B_y, T	B_z, T	B_{xx}, T/m	B_{xy}, T/m	B_{xz}, T/m	B_{yy}, T/m	B_{yz}, T/m	B_{zz}, T/m
1	0.0169	0	−0.0103	0.0162	0	−0.0318	−0.0190	0	0.0029
2	.0106	.0132	↓	−.0054	.0172	−.0196	.0024	−.0247	↓
3	−.0038	.0165	↓	−.0173	−.0076	.0070	.0144	−.0310	↓
4	−.0153	.0073	↓	.0095	−.0139	.0286	−.0125	−.0136	↓
5	−.0153	−.0073	↓	.0095	.0139	.0286	−.0125	.0136	↓
6	−.0038	−.0165	↓	−.0173	.0076	.0070	.0144	.0310	↓
7	.0106	−.0132	↓	−.0054	−.0172	−.0196	.0024	.0247	↓

(c) Electromagnet second-order gradients

Electromagnet	$B_{(xx)x}$, T/m/m	$B_{(xy)x}$, T/m/m	$B_{(xz)x}$, T/m/m	$B_{(xy)y}$, T/m/m	$B_{(xy)z}$, T/m/m	$B_{(xz)z}$, T/m/m
1	−0.0176	0	−0.0694	−0.0400	0	0.0570
2	−.0499	−.0002	−.0048	.0142	−.0512	.0356
3	.0254	−.0340	.0305	−.0129	.0226	−.0127
4	.0333	.0189	−.0494	.0187	.0414	−.0514
5	.0333	−.0189	−.0494	.0187	−.0414	−.0514
6	.0254	.0340	.0305	−.0129	−.0226	−.0127
7	−.0499	.0002	−.0048	.0142	.0512	.0356

Table A5. Eight-Coil Configuration

(a) Electromagnet parameters

Electromagnet outer radius, m	0.339
Electromagnet inner radius, m	0.152
Electromagnet height, m	0.433
Location radius, m	0.952
Maximum current density, A/cm^2	1991.83

(b) Electromagnet fields and first-order gradients

Electromagnet	B_x, T	B_y, T	B_z, T	B_{xx}, T/m	B_{xy}, T/m	B_{xz}, T/m	B_{yy}, T/m	B_{yz}, T/m	B_{zz}, T/m
1	0.0144	0	−0.0074	0.0160	0	−0.0248	−0.0150	0	−0.0010
2	.0102	.0102	↓	−.0003	.0156	−.0174	.0003	−.0174	↓
3	0	.0144		−.0150	0	0	.0160	−.0248	
4	−.0102	.0102		−.0003	−.0156	.0174	.0003	−.0174	
5	−.0144	0		.0160	0	.0248	−.0150	0	
6	−.0102	−.0102		.0003	.0156	.0174	.0003	.0174	
7	0	−.0144		−.0150	0	0	.0160	.0248	
8	.0102	−.0102		.0003	−.0156	−.0174	.0003	.0174	

(c) Electromagnet second-order gradients

Electromagnet	$B_{(xx)x}$, T/m/m	$B_{(xy)x}$, T/m/m	$B_{(xz)x}$, T/m/m	$B_{(xy)y}$, T/m/m	$B_{(xy)z}$, T/m/m	$B_{(xz)z}$, T/m/m
1	−0.0046	0	−0.0599	−0.0326	0	0.0367
2	−.0363	.0099	−.0167	.0099	−.0429	.0259
3	0	−.0326	.0257	0	0	0
4	.0363	.0099	−.0167	−.0099	.0429	−.0259
5	.0046	0	−.0599	.0326	0	−.0367
6	.0363	−.0099	−.0167	−.0099	−.0429	−.0259
7	0	.0326	.0257	0	0	0
8	−.0363	−.0099	−.0167	.0099	.0429	.0259

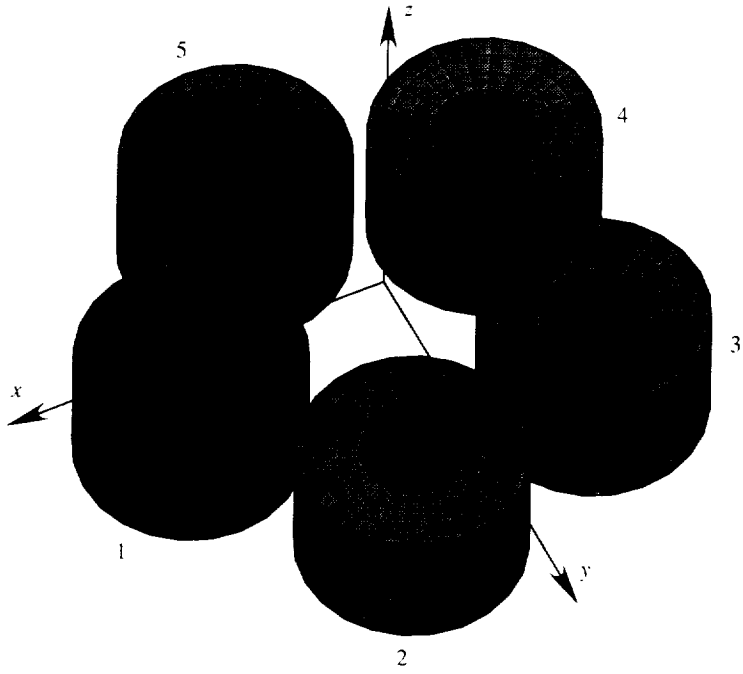

Figure A1. Five-coil configuration.

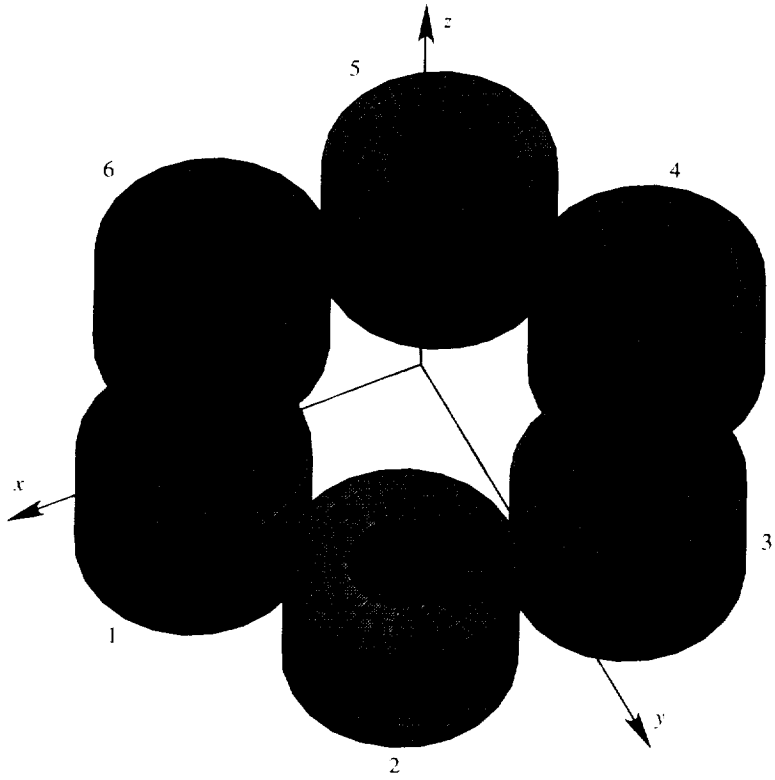

Figure A2. Six-coil configuration.

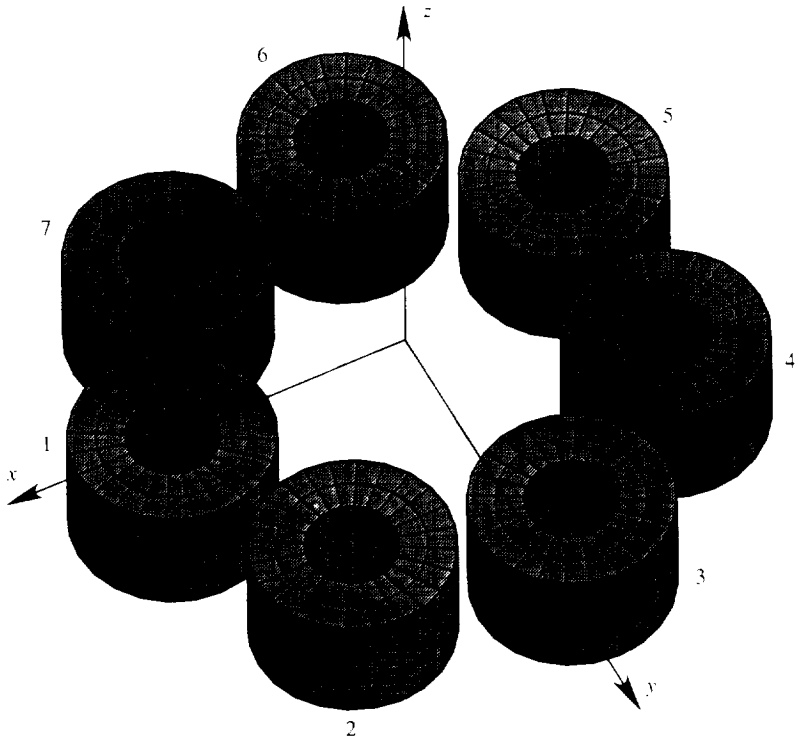

Figure A3. Seven-coil configuration.

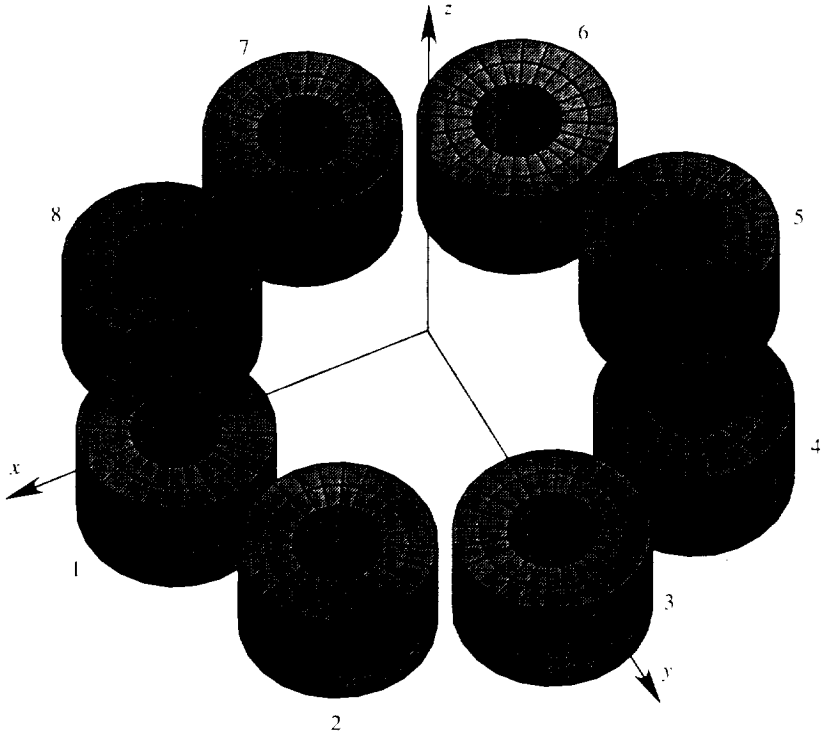

Figure A4. Eight-coil configuration.

References

1. Groom, Nelson J.: Description of the Large Gap Magnetic Suspension System (LGMSS) Ground-Based Experiment. *Technology 2000*, NASA CP-3109, Volume 2, 1991, pp. 365–377.

2. Groom, Nelson J.: *Analytical Model of a Five Degree of Freedom Magnetic Suspension and Positioning System.* NASA TM-100671, 1989.

3. Groom, Nelson J.; and Schaffner, Philip R.: *An LQR Controller Design Approach for a Large Gap Magnetic Suspension System (LGMSS).* NASA TM-101606, 1990.

4. Penrose, R.: A Generalized Inverse for Matrices. *Proc. Cambridge Philos. Soc.*, vol. 51, 1955, pp. 406–413.

5. Britcher, C. P.: *Some Aspects of Wind Tunnel Magnetic Suspension Systems With Special Application at Large Physical Scales.* NASA CR-172154, 1983.

6. Takahashi, Yasundo; Rabins, Michael J.; and Auslander, David M.: *Control and Dynamic Systems.* Addison-Wesley Publ. Co., c.1970.

7. *The VF/GFUN Reference Manual.* VF068894, Vector Fields Limited, June 20, 1988.

8. Boom, R. W.; Abdelsalam, M. K.; Eyssa, Y. M.; and McIntosh, G. E.: *Repulsive Force Support System Feasibility Study.* NASA CR-178400, 1987.

Table 1. Nonzero Eigenvalues and Eigenvectors for Five-Coil Configuration With Only B_{xz} Present

States	Mode 1 eigenvalues	Mode 2 eigenvalues
	$+/-$ 7.7995 rad/sec	$+/-$ 7.7995i rad/sec
	Mode 1 eigenvectors	Mode 2 eigenvectors
$\Omega_{\bar{y}}$	$+/+$ 1.000	$+/+$ 1.000
$\Omega_{\bar{z}}$	0	0
θ_y	$+/-$ 0.128	$-/+$ 0.128i
θ_z	0	0
$V_{\bar{x}}$	$-/-$ 0.161	$+/+$ 0.161
$V_{\bar{y}}$	0	0
$V_{\bar{z}}$	0	0
x	$-/+$ 0.021	$-/+$ 0.021i
y	0	0
z	0	0

Table 2. Uncontrolled Fields and Gradients for Five-Coil Configuration

B_x, T	-0.0419
B_{yy}, T/m	-0.0002
B_{yz}, T/m	0
B_{zz}, T/m	0
$B_{(xx)x}$, T/m/m	0.1842
$B_{(xx)y}$, T/m/m	0
$B_{(xx)z}$, T/m/m	0.0003
$B_{(xy)x}$, T/m/m	0
$B_{(xy)y}$, T/m/m	0.0615
$B_{(xy)z}$, T/m/m	0
$B_{(xz)x}$, T/m/m	0.0003
$B_{(xz)y}$, T/m/m	0
$B_{(xz)z}$, T/m/m	-0.2473

Table 3. Nonzero Eigenvalues and Eigenvectors for Five-Coil Configuration With Only B_{xz} and B_x Present

States	Mode 1 eigenvalues +/− 13.596 rad/sec Mode 1 eigenvectors	Mode 2 eigenvalues +/− 1.474i rad/sec Mode 2 eigenvectors	Mode 3 eigenvalues +/− 12.839 rad/sec Mode 3 eigenvectors
$\Omega_{\bar{y}}$	+/+ 1.000	+/+ 1.000	0
$\Omega_{\bar{z}}$	0	0	+/+ 1.000
θ_y	+/− 0.074	−/+ 0.223i	0
θ_z	0	0	+/− 0.078
$V_{\bar{x}}$	−/− 0.053	+/+ 0.490	0
$V_{\bar{y}}$	0	0	0
$V_{\bar{z}}$	0	0	0
x	−/+ 0.004	−/+ 0.109i	0
y	0	0	0
z	0	0	0

Table 4. Nonzero Eigenvalues and Eigenvectors for Five-Coil Configuration With All Nonzero Fields and Gradients Present

States	Mode 1 eigenvalues +/− 13.669 rad/sec Mode 1 eigenvectors	Mode 2 eigenvalues +/− 1.794i rad/sec Mode 2 eigenvectors	Mode 3 eigenvalues +/− 12.839 rad/sec Mode 3 eigenvectors	Mode 4 eigenvalues +/− 5.05i rad/sec Mode 4 eigenvectors	Mode 5 eigenvalues +/− 2.505 rad/sec Mode 5 eigenvectors
$\Omega_{\bar{y}}$	+/+ 1.000	+/+ 1.000	0	−/− 0.003	0
$\Omega_{\bar{z}}$	0	0	+/+ 1.000	0	+/+ 0.0.75
θ_y	+/− 0.073	−/+ 0.7557i	0	+/− 0.001i	0
θ_z	0	0	+/− 0.078	0	+/− 0.002
$V_{\bar{x}}$	−/− 0..758	+/+ 0.4.75	0	−/− 0.001	0
$V_{\bar{y}}$	0	0	0	0	+/+ 1.000
$V_{\bar{z}}$	0	+/+ 0.001	0	+/+ 1.000	0
x	−/+ 0.004	−/+ 0.248i	0	0	0
y	0	0	0	0	+/− 0.399
z	0	0	0	−/+ 0.199i	0

Table 5. Uncontrolled Fields and Gradients for Six-Coil Configuration

B_x, T	−0.0478
B_{yy}, T/m	0
B_{yz}, T/m	0
B_{zz}, T/m	0
$B_{(xx)x}$, T/m/m	0.1498
$B_{(xx)y}$, T/m/m	0
$B_{(xx)z}$, T/m/m	0
$B_{(xy)x}$, T/m/m	0
$B_{(xy)y}$, T/m/m	0.0503
$B_{(xy)z}$, T/m/m	0
$B_{(xz)x}$, T/m/m	0
$B_{(xz)y}$, T/m/m	0
$B_{(xz)z}$, T/m/m	−0.2001

Table 6. Nonzero Eigenvalues and Eigenvectors for Six-Coil Configuration With All Nonzero Fields and Gradients Present

States	Mode 1 eigenvalues	Mode 2 eigenvalues	Mode 3 eigenvalues	Mode 4 eigenvalues	Mode 5 eigenvalues
	+/− 14.402 rad/sec	+/− 1.993i rad/sec	+/− 13.717 rad/sec	+/− 4.520i rad/sec	+/− 2.267 rad/sec
	Mode 1 eigenvectors	Mode 2 eigenvectors	Mode 3 eigenvectors	Mode 4 eigenvectors	Mode 5 eigenvectors
$\Omega_{\bar{y}}$	+/+ 1.000	+/+ 1.000	0	0	0
$\Omega_{\bar{z}}$	0	0	+/+ 1.000	0	0
θ_y	+/− 0.069	−/+ 0.502i	0	0	0
θ_z	0	0	+/− 0.073	0	0
$V_{\bar{x}}$	−/− 0.051	+/+ 0.509	0	0	0
$V_{\bar{y}}$	0	0	0	0	+/+ 1.000
$V_{\bar{z}}$	0	0	0	+/+ 1.000	0
x	−/+ 0.004	−/+ 0.255i	0	0	0
y	0	0	0	0	+/− 0.441
z	0	0	0	−/+ 0.221i	0

Table 7. Uncontrolled Fields and Gradients for Seven-Coil Configuration

B_x, T	-0.0514
B_{yy}, T/m	-0.0001
B_{yz}, T/m	0
B_{zz}, T/m	0
$B_{(xx)x}$, T/m/m	0.1305
$B_{(xx)y}$, T/m/m	0
$B_{(xx)z}$, T/m/m	-0.0002
$B_{(xy)x}$, T/m/m	0
$B_{(xy)y}$, T/m/m	0.0438
$B_{(xy)z}$, T/m/m	0
$B_{(xz)x}$, T/m/m	-0.0002
$B_{(xz)y}$, T/m/m	0
$B_{(xz)z}$, T/m/m	-0.1728

Table 8. Nonzero Eigenvalues and Eigenvectors for Seven-Coil Configuration With All Nonzero Fields and Gradients Present

	Mode 1 eigenvalues	Mode 2 eigenvalues	Mode 3 eigenvalues	Mode 4 eigenvalues	Mode 5 eigenvalues
	$+/-$ 14.834 rad/sec	$+/-$ 2.139i rad/sec	$+/-$ 14.218 rad/sec	$+/-$ 4.201i rad/sec	$+/-$ 2.116 rad/sec
States	Mode 1 eigenvectors	Mode 2 eigenvectors	Mode 3 eigenvectors	Mode 4 eigenvectors	Mode 5 eigenvectors
$\Omega_{\bar{y}}$	$+/+$ 1.000	$+/+$ 1.000	0	$+/+$ 0.002	0
$\Omega_{\bar{z}}$	0	0	$+/+$ 1.000	0	$+/+$ 0.003
θ_y	$+/-$ 0.067	$-/+$ 0.468i	0	$-/+$ 0.001	0
θ_z	0	0	$+/-$ 0.070	0	$+/-$ 0.001
$V_{\bar{x}}$	$-/-$ 0.047	$+/+$ 0.548	0	$+/+$ 0.001	0
$V_{\bar{y}}$	0	0	0	0	$+/+$ 1.000
$V_{\bar{z}}$	0	$-/-$ 0.001	0	$+/+$ 1.000	0
x	$-/+$ 0.003	$-/+$ 0.256i	0	0.001	0
y	0	0	0	0	$+/-$ 0.473
z	0	0	0	$-/+$ 0.238i	0

Table 9. Uncontrolled Fields and Gradients for Eight-Coil Configuration

B_x, T	−0.0560
B_{yy}, T/m	0
B_{yz}, T/m	0
B_{zz}, T/m	0
$B_{(xx)x}$, T/m/m	0.1083
$B_{(xx)y}$, T/m/m	0
$B_{(xx)z}$, T/m/m	0
$B_{(xy)x}$, T/m/m	0
$B_{(xy)y}$, T/m/m	0.0365
$B_{(xy)z}$, T/m/m	0
$B_{(xz)x}$, T/m/m	0
$B_{(xz)y}$, T/m/m	0
$B_{(xz)z}$, T/m/m	−0.1425

Table 10. Nonzero Eigenvalues and Eigenvectors for Eight-Coil Configuration With All Nonzero Fields and Gradients Present

	Mode 1 eigenvalues	Mode 2 eigenvalues	Mode 3 eigenvalues	Mode 4 eigenvalues	Mode 5 eigenvalues
	+/− 15.384 rad/sec	+/− 2.311i rad/sec	+/− 14.841 rad/sec	+/− 3.814i rad/sec	+/− 1.930 rad/sec
States	Mode 1 eigenvectors	Mode 2 eigenvectors	Mode 3 eigenvectors	Mode 4 eigenvectors	Mode 5 eigenvectors
$\Omega_{\bar{y}}$	+/+ 1.000	+/+ 1.000	0	0	0
$\Omega_{\bar{z}}$	0	0	+/+ 1.000	0	0
θ_y	+/− 0.065	−/+ 0.433i	0	0	0
θ_z	0	0	+/− 0.067	0	0
$V_{\bar{x}}$	−/− 0.043	+/+ 0.598	0	0	0
$V_{\bar{y}}$	0	0	0	0	+/+ 1.000
$V_{\bar{z}}$	0	0	0	+/+ 1.000	0
x	−/+ 0.003	−/+ 0.259i	0	0	0
y	0	0	0	0	+/− 0.518
z	0	0	0	−/+ 0.262i	0

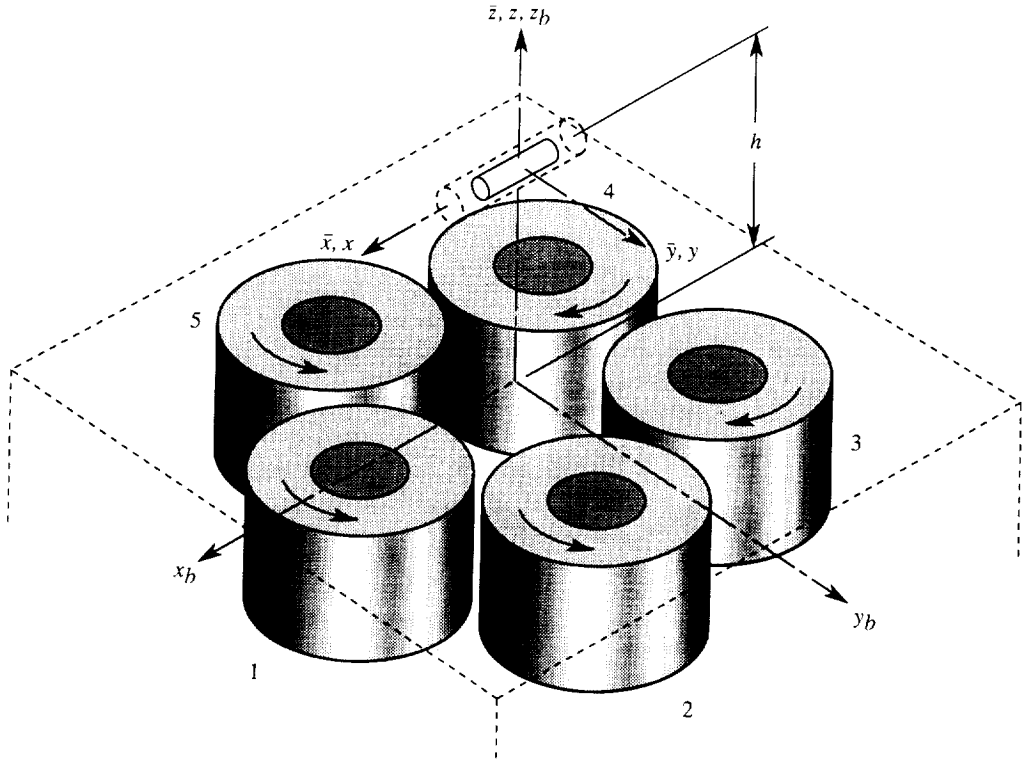

Figure 1. Initial alignment of coordinate system for Large-Gap Magnetic Suspension System.

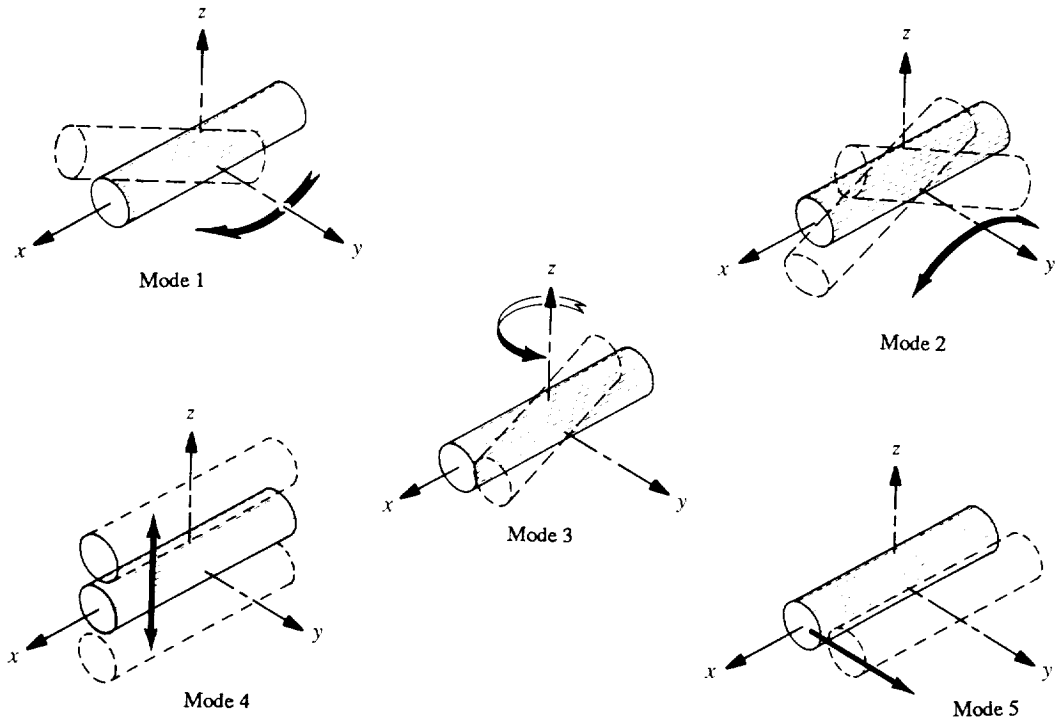

Figure 2. Open-loop modes for five-coil configuration.

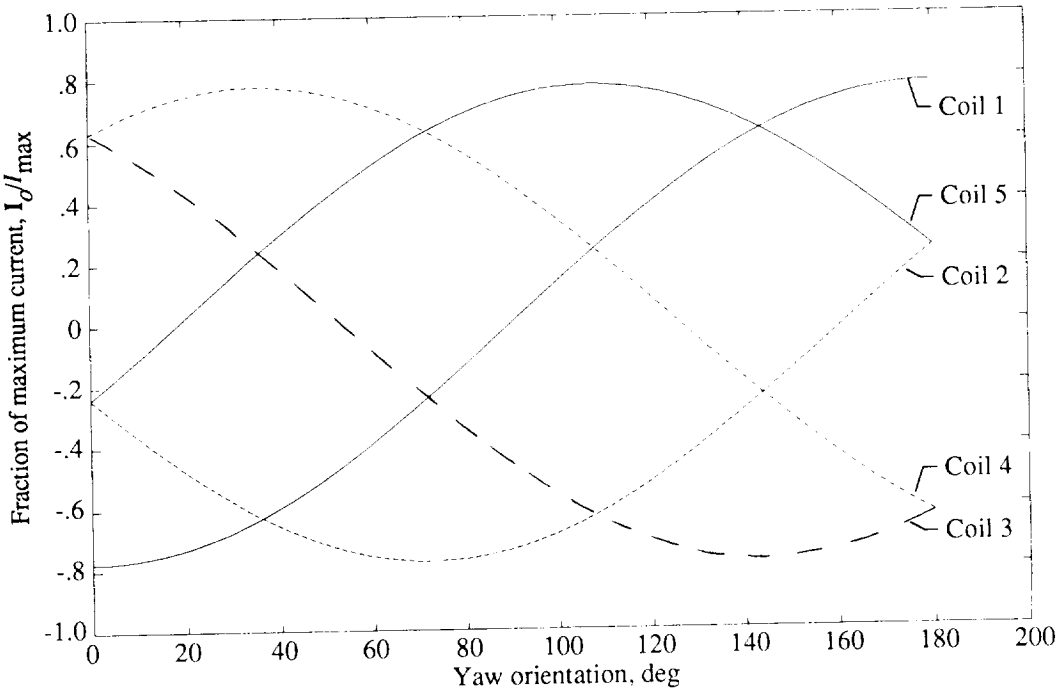

Figure 3. Variation of equilibrium suspension currents with yaw for five-coil configuration.

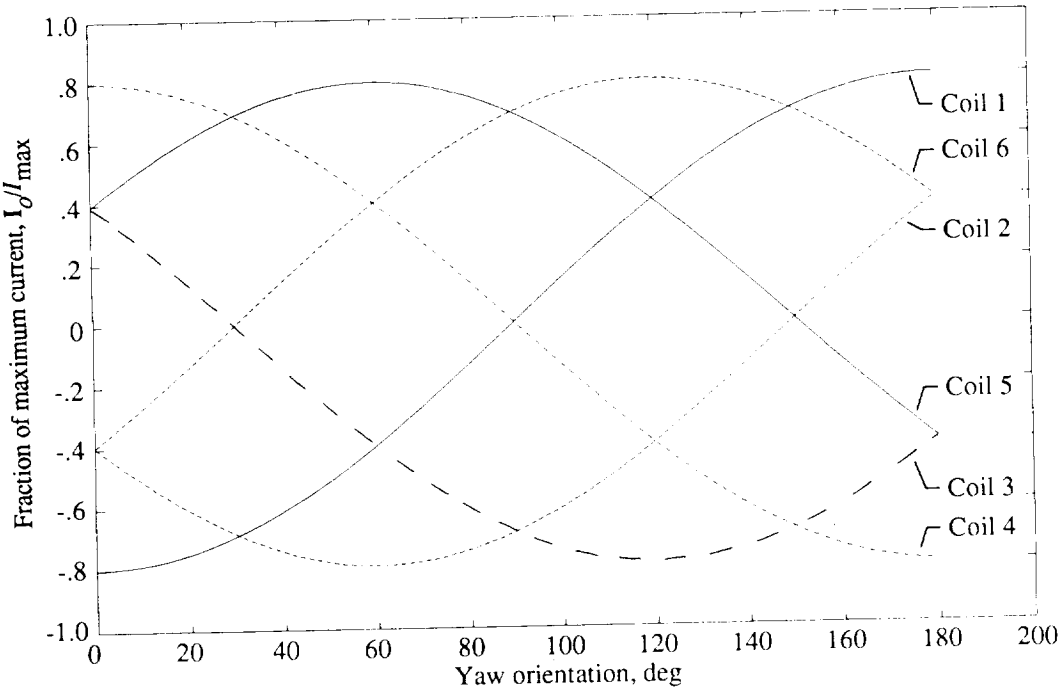

Figure 4. Variation of equilibrium suspension currents with yaw for six-coil configuration.

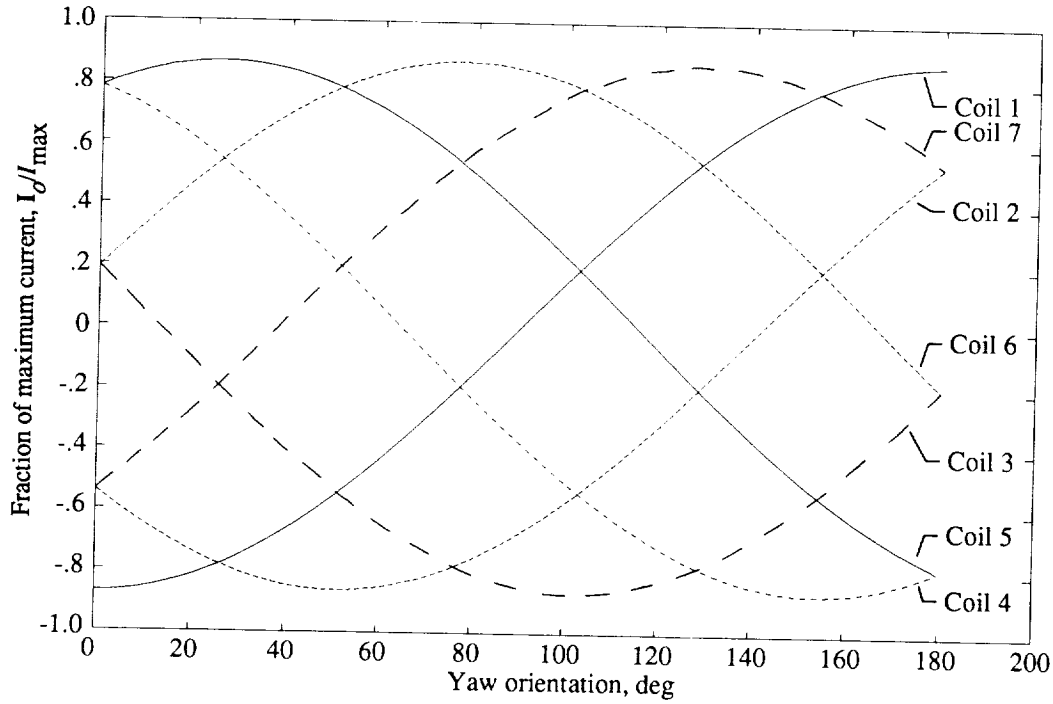

Figure 5. Variation of equilibrium suspension currents with yaw for seven-coil configuration.

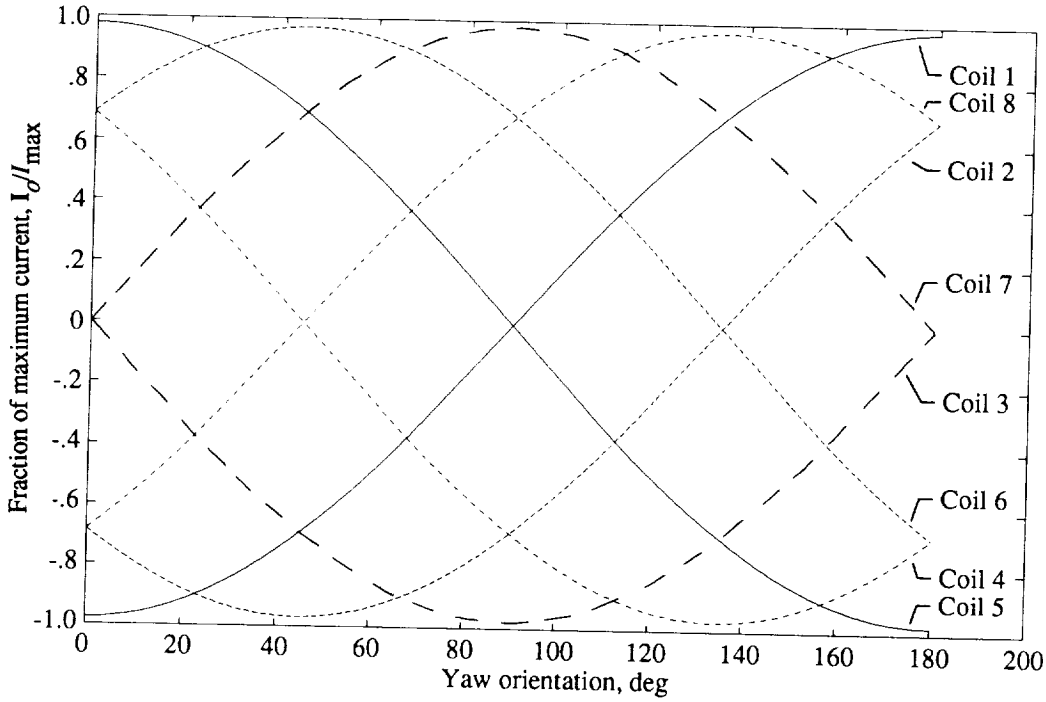

Figure 6. Variation of equilibrium suspension currents with yaw for eight-coil configuration.